Slov Vet Res
DOI 10.26873/SVR-2205-2025
UDC 599.723.12:57.082.14:616.728:591.476:543.442
Pages: 157–68

Original Research Article

New Insights Into the Horse Stifle Joint Through 3D Computed Tomography, Scanning Electron Microscopy, and Scanning Electron Microscopy-Energy Dispersive X-ray Analysis

Key words

horse;
stifle;
3D CT;
sectional anatomy;
SEM;
SEM-EDX

Mohamed A. M. Alsafy[1]*, Ahmed K. S. El-Garhy[2], Ismail Abo-Ghanima[3], Ahmed G. Nomir[2], Samir A. A. El-Gendy[1]

[1]Anatomy and Embryology Department, Faculty of Veterinary Medicine, Alexandria University, Abis 10th P.O. 21944, Alexandria, [2]Department of Anatomy and Embryology, [3]Department of Physiology, Faculty of Veterinary Medicine, Damanhour University, Damanhour 22511, Egypt

***Corresponding author:** mohamed.alsafy@alexu.edu.eg

Abstract: The study design was prospective and descriptive of the horse stifle joint using CT, sectional anatomy, SEM, and EDX analysis. The 3D rendered-volume reconstruction CT of the horse's stifle joint allows good visualization of the large and small bony structures and ligaments, or menisci. In addition to the sagittal CT section and subsequent CT bone window cross sections, which provided detailed images of bone structures, ligaments, and muscles, the sectional CT was matched with cross and sagittal anatomical sections. The horse's stifle joint is described using SEM and EDX analysis. The synovial membrane had varied synovial villi in length and shape: long and short tongue shapes with different tip shapes and dome-shaped, in addition to single or branched folds. The scratched surface revealed a network of collagen fibers arranged in various directions, layers, and deep synoviocytes. SEM-EDX Spectra identified the following items in the stifle joint's meniscus and ligaments: The sample contained carbon, oxygen, nitrogen, sulfur, calcium, and phosphorus, with selenium replaced by sulfur at the meniscus. Four specimens were examined to determine their carbon and oxygen percentages. Calcium and phosphorus levels were measured, with the highest concentrations in the meniscus and the lowest in the collateral and patellar ligaments. The percentage of sulfur was determined, and ligaments had a higher percentage than menisci, particularly at the cruciate ligaments, whereas menisci contained silicon. Knowledge of the stifle joint's macro- and microscopic normal anatomy obtained through 3D CT, SEM, and EDX is a good guide and reference for determining the horse stifle's bony and soft tissue structures and microstructures, as well as the chemical structure of the synovial membrane, ligaments, and menisci.

Received: 3 March 2025
Accepted: 6 April 2025

Introduction

The stifle is a condylar synovial joint. It is a compound joint in structure and function (1, 2). Ligaments are tough, fibrous con-nective tissues that connect bones and provide support while limiting excessive movement. They are essential for maintaining the stability, integrity, and proper alignment of the stifle joint (3). The stifle's primary stabilizers are the cranial and caudal cruciate ligaments, which limit cranial translation and rotation of the tibia (4, 5).

The stifle joint affection is a significant cause of lameness in horse's hind limb (6, 7, 8). Because of their clinical significance, anatomically normal and pathologically altered stifle joints have been extensively studied using radiography

and ultrasonography (9, 10). Horses frequently experience hindlimb lameness and, stifle injuries are among the leading causes of this ailment (11, 12). The stifle joint, a major weight-bearing joint in the horse's hindlimb, is vulnerable to various soft tissue and ligament injuries (11). Stifle joint clinical problems usually necessitate surgical intervention in case of meniscal tears, patellar dislocation, frac-tures, and ligament sprains (13). However, appropriately diagnos-ing these specific stifle injuries remains a significant difficulty for equine veterinarians (7, 14, 15).

Computed tomography (CT) is an effective technique for produc-ing good sectional anatomical images with no superimposition of structures (16, 17). Furthermore, three-dimensional CT (3D-CT) is an effective diagnostic tool for determining the osseous anatomi-cal structures and distinguishing ligaments (18, 19, 20, 21).

Scanning electron microscopy was widely used to determine the structures and whole cell shapes of the synovial membrane and synoviocytes of an equine's joint capsule (22, 23). Although nu-merous reviews have detailed their structure, molecular composi-tion, and biomechanical properties, little attention has been paid to their trace element content (24, 25, 26). The synovial mem-brane consisted of a connective tissue layer lined by synovial cells on the surface facing the articular cavity, with two types of syno-viocytes (27). Ligaments and tendons were the main structures that promoted joint movement and stability (28). The presence of trace elements is related to their molecular composition and biomechanical properties (29). Ligaments and tendons were primarily rich in calcium, sulfur, and phosphorus, though notable differences existed between tendons and ligaments (26, 28).

The stifle joint was the largest and most compound joint in the limbs. The anatomical description of its structure has been re-ported using many detailed techniques in previously published articles, such as anatomical description, computed tomography, ultrasound, and MRI (18, 30, 31, 32, 33, 34, 35, 36).

The current study primarily focused on 3D CT reconstruction, scanning electron microscopy of synovial villi, and comparing the composition of trace minerals in various ligaments and menisci of the stifle joint in horses.

Materials and methods

Samples

Four adult horses were euthanized for other reasons unrelated to this study; the horses are owned and have been provided for teaching in the Department of Anatomy and Embryology. Horses were given a subcutaneous injection of 2 ampoules of the antico-agulant CLEXAN 20 and intravenously injected with 3 liters of sodium chloride solution to aid in thorough bleeding. Euthanasia was undertaken under general anesthesia by veterinary sur-geons via intravenous injection of 10 mg/kg thiopental sodium (EPICO, Egypt) after premedication with 1 mg/kg xylazine hydro-chloride (Xylaject; Egypt). Following euthanasia, the animals bled from the common carotid artery. All hindlimbs were disarticulat-ed at the hip joint.

Computed tomography (CT)

Four fresh hind limbs from horses underwent computed tomog-raphy 45 minutes after death. The stifle joint was scanned using a Toshiba Asteion CT scanner, four slices, 2003. The distance between the slices taken was 0.5 cm, with a voltage range of 100 kV and 200 mA. 3D reconstruction from the transverse and sagit-tal computed tomography (37, 38); in the end, all images were stacked together sequentially to obtain a 3D image model of the inspected object. The reconstruction algorithm was done with Octopus software and converted to digital imaging and commu-nications in medicine (DICOM format) (19, 39, 40, 41).

Cadaver gross sections

Four fresh hind limbs from adult horses were tightly placed in adhesive tape to prevent air entrapment and distal slippage of soft tissue structures. The freshly collected limbs were frozen (-12°C) for two days. After preservation, using an electric wood tray saw, the frozen hind limbs were carefully sliced (one limb cut transverse and one limb cut sagittal) at the stifle joint region. The slices were cut to a uniform thickness of 2 cm. Each slice was assigned a number for identification purposes. The slices were gently cleaned of debris with water and a light brushing. The cleaned slices were then promptly photographed. These slices were imaged using a Canon EOS 700D digital camera and matched with the correlated CT images (21, 23, 42).

Scanning electron microscopy (SEM)

Two horses (4 fresh hind limbs from adult horses aged 10 years old) were used to collect samples for SEM from both right and left limbs. The samples from the synovial membrane were fixed in a solution containing glutaraldehyde, formaldehyde, and sodium cacodylate (43, 44). Subsequently, they were rinsed in a sodium cacodylate solution with sucrose, treated with tannic acid, and dehydrated gradually using increasingly concentrated ethanol solutions. Afterward, the samples were desiccated with carbon dioxide, affixed to mounts, and coated with a gold-palladium mixture. The prepared samples were imaged using a JEOL JSM-IT200 SEM (45, 46, 47).

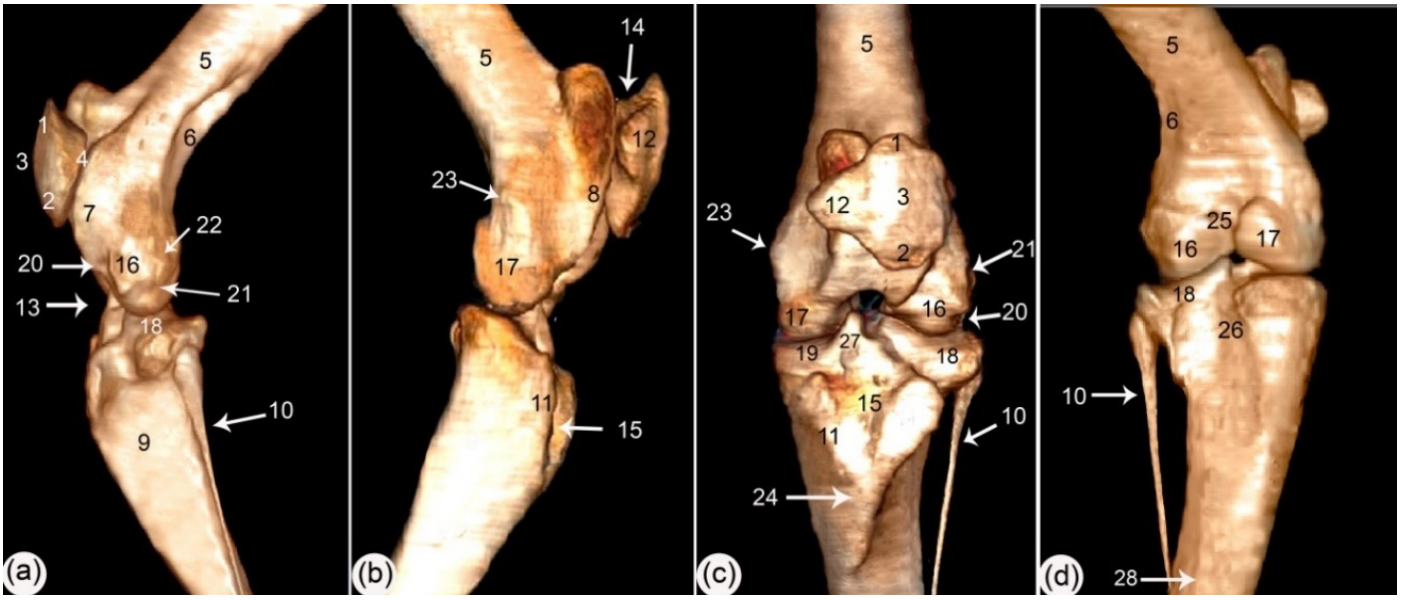

Figure 1: 3D render volume reconstruction of CT of the stifle joint bony structures. (a) lateral view. (b) medial view. (c) cranial view. (d) caudal view

1. base of the patella (*Basis patellae*); 2. apex of the patella (*Apex patellae*); 3. cranial face (*Facies cranialis*); 4. articular surface (*Facies articu-laris*); 5. Femur (*Os femoris*); 6. supracondylar fossa (*Fossa supracondylaris*); 7. lateral trochlear ridge; 8. medial trochlear ridge; 9. Tibia; 10. fibula; 11. tibial tuberosity (*Tuberositas tibiae*); 12-medial angle of patella; 13. femorotibial joint; 14. femoropatellar joint; 15-tibial sulcus (*Sulcus tuberositatis tibiae*); 16. lateral femoral condyle (*Condylus lateralis*); 17. medial femoral condyle (*Condylus medialis*); 18. lateral tibial condyle (*Tibial condylus lateralis*); 19. medial tibial condyle (*Tibial condylus medialis*); 20. extensor fossa (*Fossa extensoria*); 21. popliteal fossa (*Fossa m. poplitei*); 22. lateral epicondyle (*Epicondylus lateralis*); 23. medial epicondyle (*Epicondylus medialis*); 24. tibial crest; 25. intercondyloid fossa (*Fossa intercondylaris*); 26. popliteal notch (*Incisura poplitea*); 27. intercondyloid eminence (*Emi-nentia intercondylaris*); 28. popliteal lines (*Linea m. poplitei*).

Scanning electron microscopy-Energy Dispersive X-Ray Analysis (SEM-EDX)

The patellar ligament, collateral ligament, cruciate ligament, and menisci samples were analyzed and photographed with a JEOL JSM-IT200 scanning electron microscope at 20 kV. The quantification method was ZAF analysis. The sample distance from the detector was 10 mm, the real-time was 30.97 seconds, and the dead time was 3.00% (48, 49, 50). The EDX spectrometer was created at the Science Faculty, Alexandria University, Egypt.

Results

Computed tomography and sectional anatomy of the horse's stifle joint

The 3D rendered-volume reconstruction of the horse's stifle joint produced numerous images at 360 degrees, allowing for good visualization of the large and small bony structures, ligaments, and menisci (Figs. 1, 2). In addition to the sagittal CT section and subsequent CT bone window cross sections, which provided de-tailed images of the bones, the sectional CT was matched with cross and sagittal anatomical sections. Images revealed all bone structures, including the femur's distal diaphysis, condyles, trochlear ridges, intercondyloid fossa (*fossa intercondylaris*), extensor fossa (*fossa extensoria*), popliteal fossa (*fossa m. poplitei*), patel-la, tibial intercondylar eminence (*eminentia intercondylaris*), tibial tuberosity (*tuberositas tibiae*) (Figs. 3,

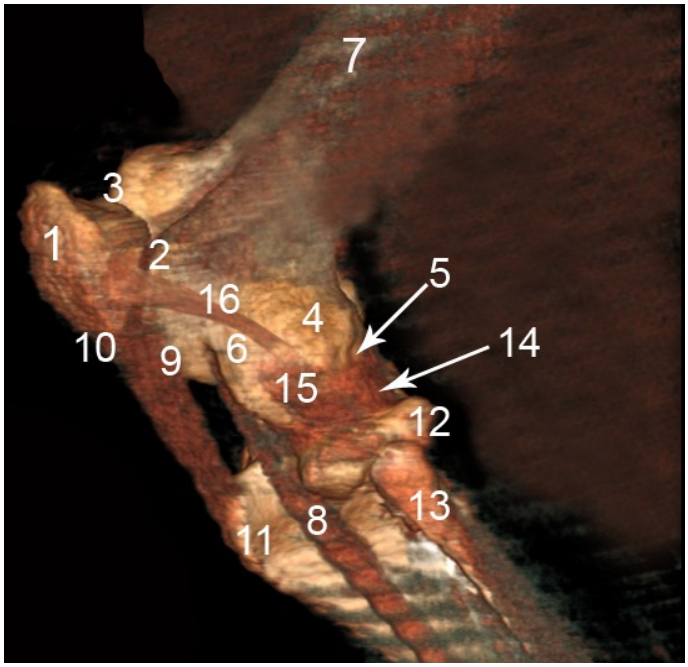

Figure 2: 3D render volume reconstruction of CT, lateral view, explains the details of the stifle joint

patella; 2. lateral trochlear ridge; 3. medial trochlear ridge; 4. lateral epicondyle (*Epicondylus lateralis*); 5. popliteal fossa (*Fossa m. pop-litei*); 6. extensor fossa (*Fossa extensoria*); 7. femur shaft (*Corpus ossis femoris*); 8. long digital extensor muscle (*Extensor digitorum longus*); 9. lateral patellar ligament (*Lig. patellae laterale*); 10. middle patellar ligament (*Lig. patellae intermedium*); 11. tibial tuberosity (*Tuberositas tibiae*); 12. lateral condyle of tibia (*Condylus medialis*); 13. fibula; 14. lateral meniscus (*Meniscus lateralis*); 15. lateral collat-eral ligament (*Lig. collaterale laterale*); 16. lateral femoropatellar ligament (*Lig. femoropatellare laterale*)

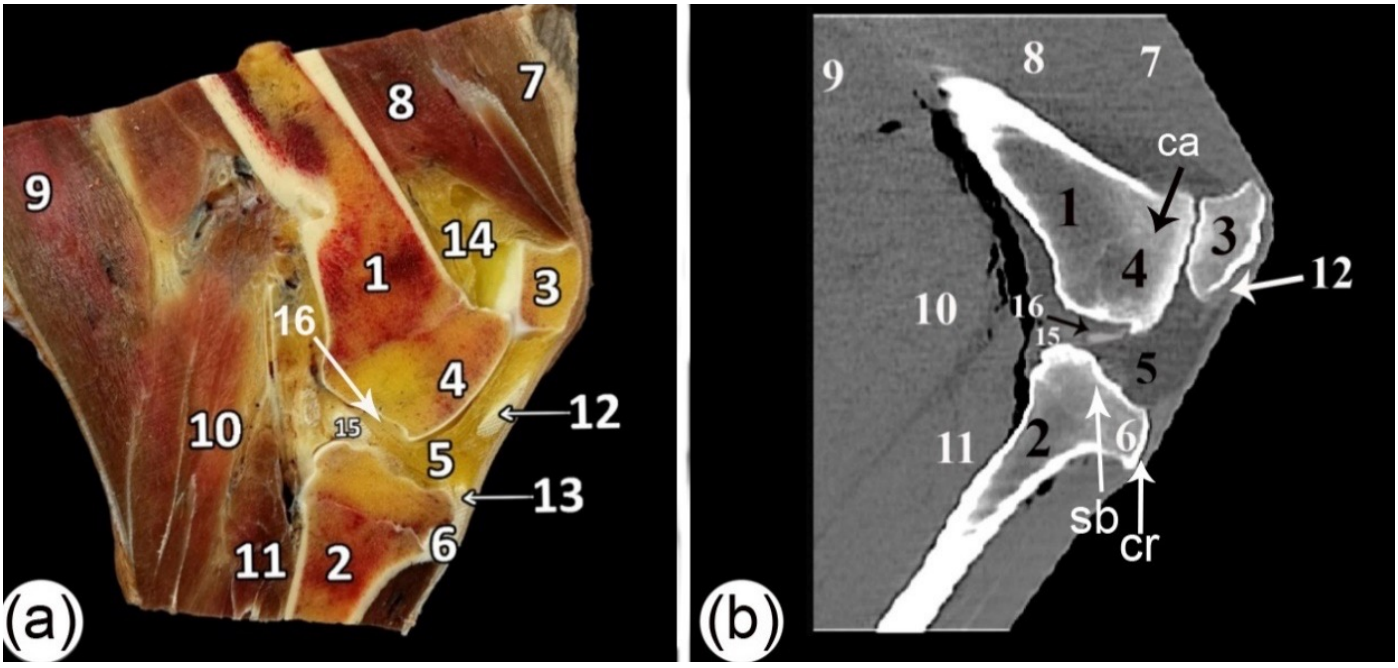

Figure 3: Sagittal sections of the stifle joint at the midline; (a) cadaver section; (b) CT scan

1. Femur (*Os femoris*); 2. tibia; 3. patella; 4. lateral ridge of the trochlear of the femur; 5. infra-patellar fat pad; 6.tibial tuberosity (*Tuberositas tibiae*); 7.rectus femoris muscle (*M. rectus femoris*); 8.vastus lateralis muscle (*M. vastus lateralis*); 9.semimembranosus muscle (*M. semi-membranosus*); 10. Lateral head of gastrocnemius muscle (*Gastrocnemius caput laterale*); 11. superficial digital flexor muscle (*M. flexor digi-torum superficialis*); 12. middle patellar ligament (*Lig. patellae intermedium*); 13. medial patellar ligament (*Lig. patellae mediale*); 14. lateral recess of the femorotibial joint; 15. caudal horn of the lateral meniscus; 16. caudal cruciate ligament (*Lig. cruciatum caudale*); (cr) cortical bone; (ca) cancellous bone (sb); subchondral bone.

4, 5, 6, 7). The infrapatellar fat pad, three patellar ligaments (*lig. patellae*), the origin of the tendinous portions of the long digital extensor muscle (*extensor digitorum longus*), and the collateral ligaments (*lig. collaterale laterale* and *lig. collaterale mediale*) of the femorotibial and fem-oropatellar joints (*articulatio femorotibialis* and *articulatio fem-oropatellaris*) were examined. The tendinous part of the popliteus muscle (*m. popliteus*), the cranial and caudal cruciate ligaments (*lig. cruciatum craniale* and *lig. cruciatum caudale*), and the me-niscotibial ligaments (*lig. meniscotibiale*) (Figs. 2, 3, 4, 5, 6, 7). In addition to explaining the patterns of the cortical, cancellous, and subchondral bones (Fig. 3).

SEM of the horse's stifle joint synovial membrane

The synovial membrane was covered with closely arranged syn-ovial villi (Fig. 8a). The villi varied in length and were classified as either long or short; the longer villi had smooth tips. The short ones had a slight wavy serration, but the surface of some villi was folded. We observed several different shapes of synovial villi, including a long tongue-like shape with a round end and a short circular and short tongue shape. Other areas of the synovial membrane's surface had folded synovial membrane; the folds were either single or branched (Fig. 8b). The synovial villi surface has a bubbling dome structure with dome-shaped synoviocytes, as well as a rough surface with microridges and pores (Fig. 8c, d). The scratched surface revealed the presence of a network of collagen fibers in various directions and layers, as well as visible deep synoviocytes (Fig. 9a, b, c, d).

SEM-EDX

The micro-elemental image of the menisci, patellar ligaments, cruciate ligament, and collateral ligament was obtained from the photon energy dispersive X-ray spectra of four specimens from two horses. EDX spectra identified the element by mass% and atom% (Figs. 10, 11, 12, 13; Table 1). We used a mass percent-age, and the EDX spectra recognized and detected the following: At our work, the SEM-EDX spectra identified the following items: menisci and various stifle joint ligaments. Carbon, oxygen, nitro-gen, sulfur, calcium, phosphorus, and silicon were replaced by sulfur in one sample of the meniscus. The calcium and phospho-rus percentages were calculated, with the menisci having the highest and the collateral and patellar ligaments having the low-est. The percentage of sulfur was higher in the ligaments than in the menisci, especially in the cruciate ligaments. The percentages of carbon and oxygen were approximately determined at four specimens and ranged from 38.7 to 42.9%, with the highest level at the menisci. Additionally, the percentages of oxygen were closely ranged from 32.6% to 36.3%, with the highest level at the cruciate ligaments. Nitrogen percentage had a higher mean at the patellar ligament.

Discussion

In our investigation, we used 3D render volume reconstruction CT of the horse's stifle joint bones, which

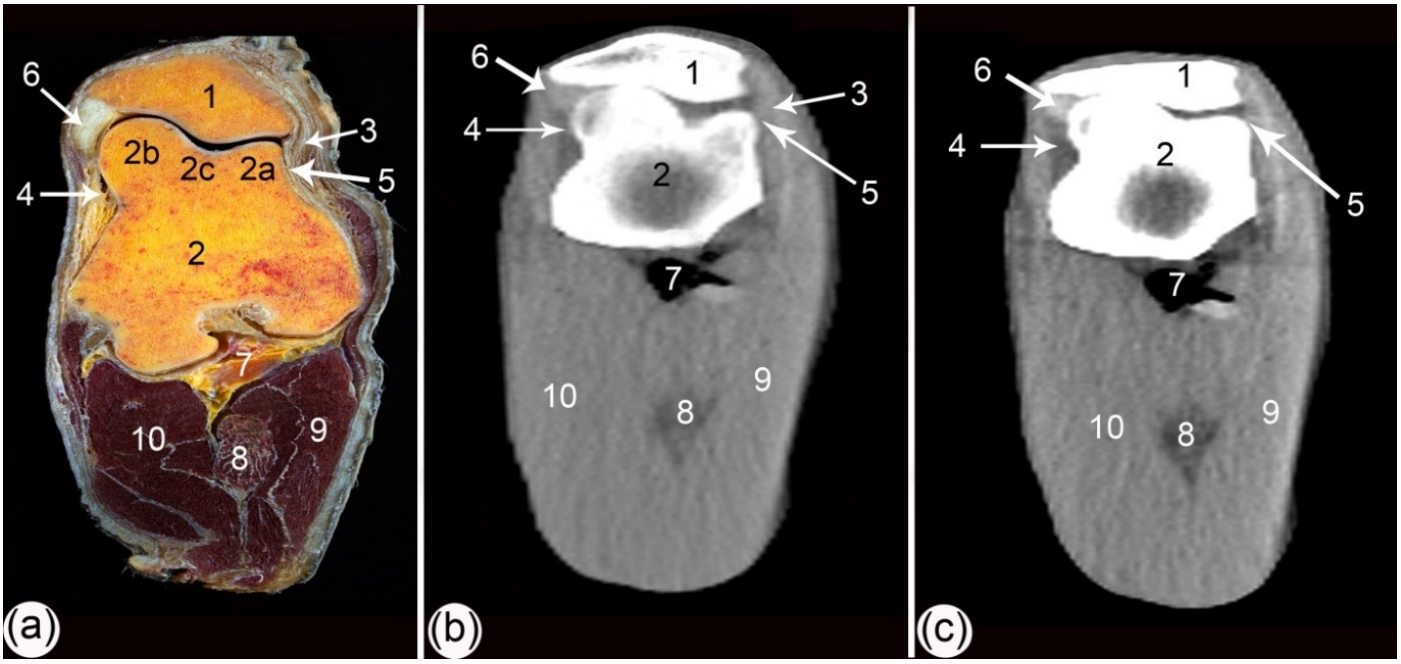

Figure 4: Cross-sections of the stifle joint proximal to the apex of the patella; (a) cadaver section; (b & c) CT scans

1. patella; 2. Femur (*Os femoris*); 2a. medial trochlear ridge; 2b. Lateral trochlear ridge; 2c. The groove of the femoral trochlear; 3. medial patellar ligament (*Lig. patellae mediale*); 4. lateral recess of femoropatellar joint; 5. medial recess of femoropatellar joint; 6. lateral patellar ligament (*Lig. collaterale laterale*); 7. joint capsule (caudal recess); 8. superficial digital flexor muscle (*M. flexor digitorum superficialis*); 9. medial head of the gastrocnemius muscle (*Gastrocnemius caput mediale*); 10. lateral head of the gastrocnemius muscle (*Gastrocnemius caput laterale*)

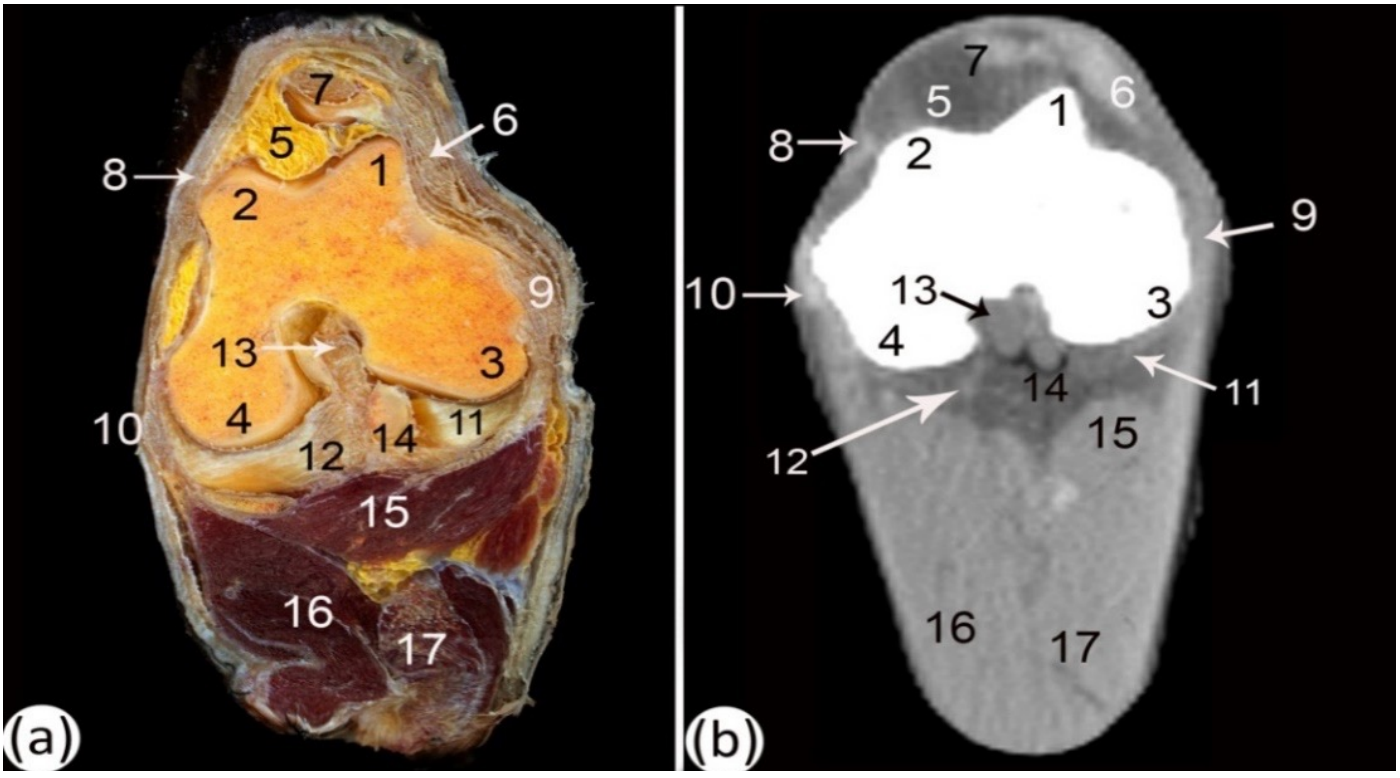

Figure 5: Cross-sections of the stifle joint through the femur intercondylar fossa; (a) cadaver section; (b) CT scan

1. medial ridge of the femoral trochlear; 2. lateral ridge of the femoral trochlear; 3. medial femoral condyle (*Condylus medialis*); 4. lateral femo-ral condyle (*Condylus lateralis*); 5. infra-patellar fat pad; 6. medial patellar ligament (*Lig. patellae mediale*); 7. middle patellar ligament (*Lig. patellae intermedium*); 8. lateral patellar ligament (*Lig. patellae laterale*); 9. medial collateral ligament (*Lig. collaterale mediale*); 10. lateral col-lateral ligament (*Lig. collaterale laterale*); 11. medial menisci (*Meniscus medialis*) 12. meniscofemoral ligament (*Lig. meniscofemorale*); 13. cranial cruciate ligament (*Lig. cruciatum craniale*); 14. caudal cruciate ligament (*Lig. cruciatum caudale*); 15. popliteus muscle (*M. popliteus*); 16. gastrocnemius muscle (*M. gastrocnemius*); 17. superficial digital flexor muscle (*M. flexor digitorum superficialis*)

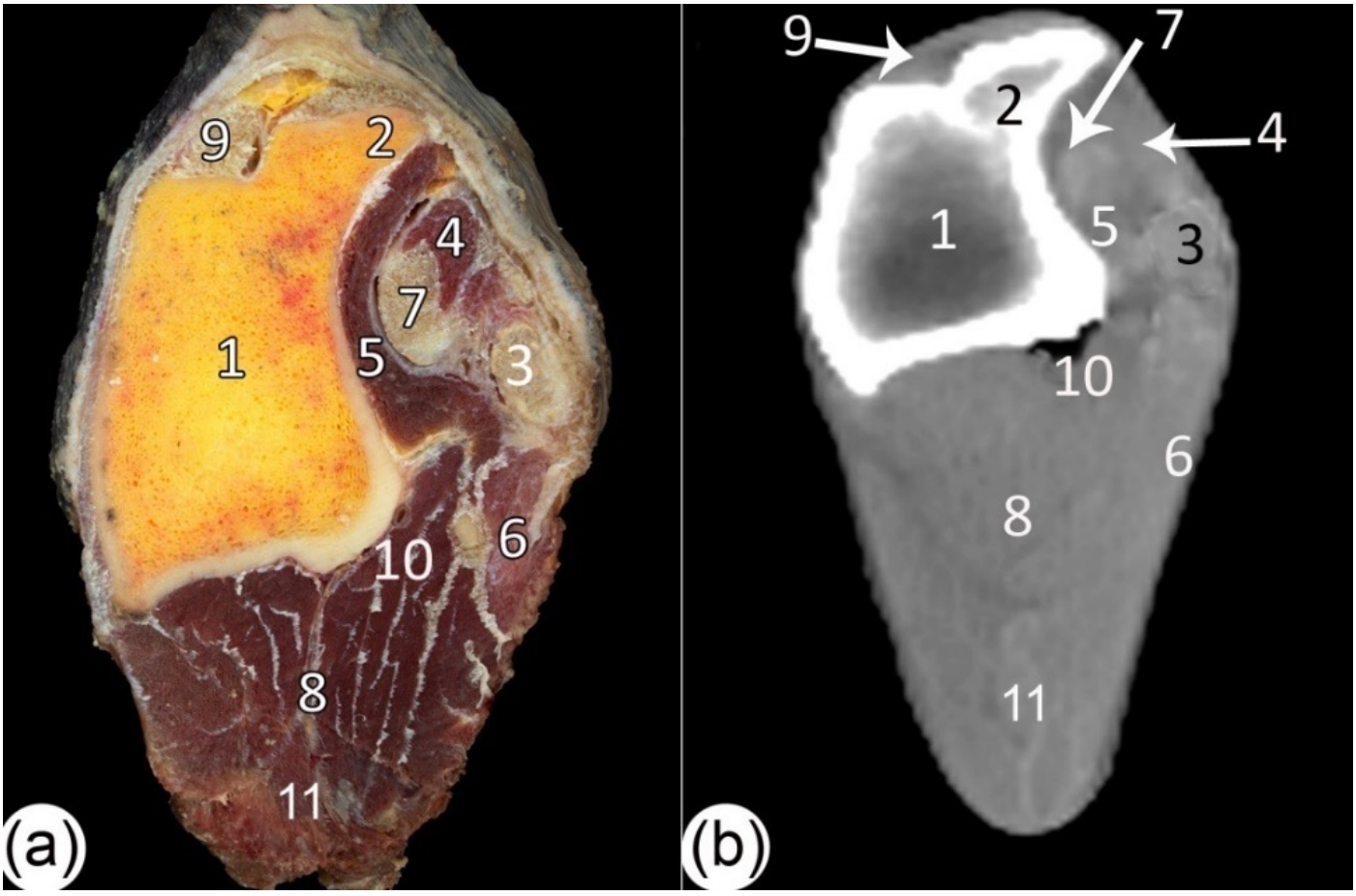

Figure 6: Cross-sections of the stifle joint at the level of the tibia proximal extremity; (a) cadaver section; (b) CT scan

1. tibia; 2. tibial crest; 3. fibula; 4. long digital extensor muscle (*M. extensor digitorum longus*); 5. tibialis cranialis muscle (*M. tibialis cranialis*); 6. lateral digital extensor muscle (*M. extensor digitorum lateralis*); 7. fibularis tertius muscle; 8. superficial digital flexor muscle (*M. flexor digitorum superficialis*); 9. middle patellar ligament (*Lig. patellae intermedium*); 10. caudal tibial artery (*A. tibialis caudalis*); 11. gastrocnemius muscle (*M. gastrocnemius*)

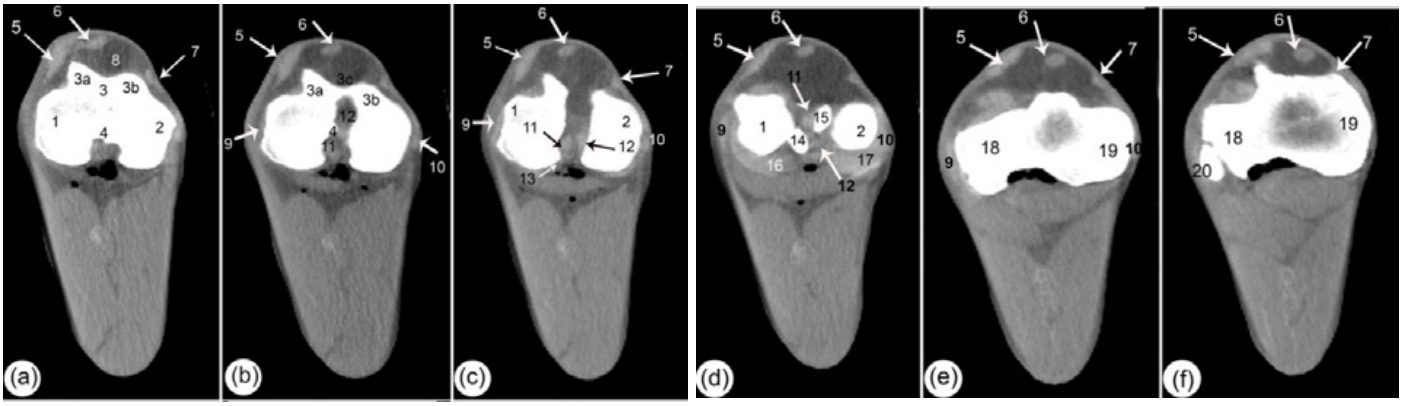

Figure 7: Transverse CT bone window scans at the femorotibial joint (Articulatio femorotibialis) (Serial sections a, b, c and d at the level of femoral condyles while e, f at the level of tibial condyles)

1. lateral femoral condyle (*Condylus lateralis*); 2. medial femoral condyle (*Condylus medialis*); 3. trochlea; 3a. lateral ridge of the femoral troch-lear; 3b. medial ridge of the femoral trochlear; 4c. trochlear groove; 5. lateral patellar ligament (*Lig. patellae laterale*); 6. middle patellar ligament (*Lig. patellae intermedium*); 7. medial patellar ligament (*Lig. patellae mediale*); 8. infra-patellar fat pad; 9. lateral collateral ligament (*Lig. collat-erale laterale*); 10. medial collateral ligament (*Lig. collaterale mediale*); 11. cranial cruciate ligament (*Lig. cruciatum craniale*); 12. caudal cruci-ate ligament (*Lig. cruciatum caudale*); 13. meniscofemoral ligament; 14. lateral tubercle of intercondyloid eminence (*Tuberculum intercon-dylare laterale*); 15. medial tubercle of intercondyloid eminence (*Tuberculum intercondylare mediale*); 16. lateral meniscus (*Meniscus lat-eralis*); 17. medial meniscus (*Meniscus medialis*); 18. lateral tibial condyle (*Condylus medialis*); 19. medial tibial condyle (*Condylus medialis*)

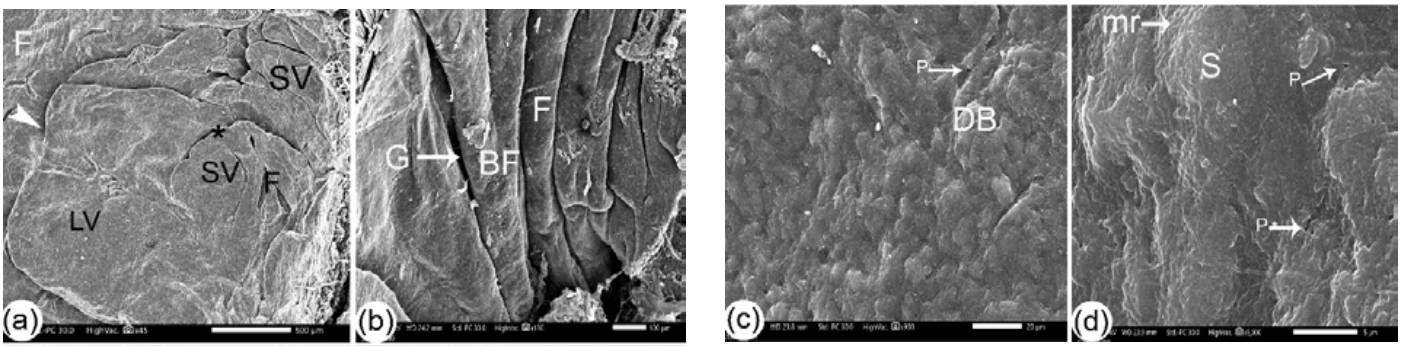

Figure 8: Scanning electron micrographs of the stifle joint synovial membrane

Long tongue-shaped villi (LV) with smooth tips (arrowhead); short circular and tongue-shaped villi (SV) with slight wavy tips (*); folds (F); branched folds (BF); dome-shaped bubbly structures (DB); dome-shaped synoviocytes (S); micro-ridges (mr); pores (P)

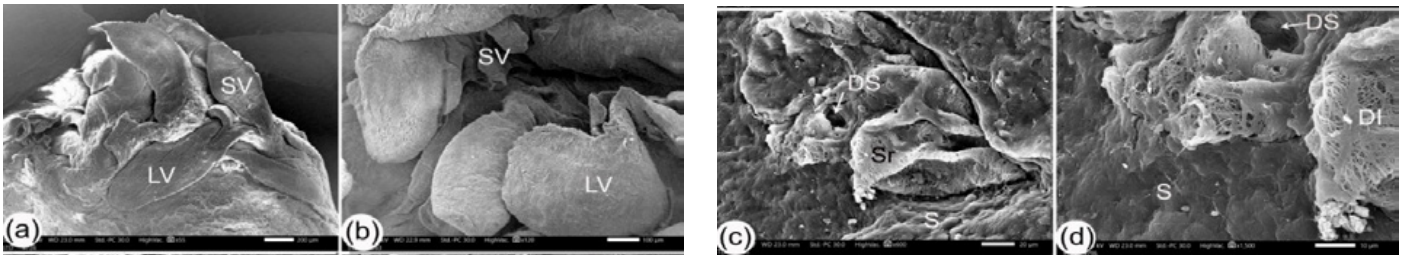

Figure 9: Scanning electron micrographs of the stifle joint synovial membrane

Long tongue-shaped villi (LV); short tongue-shaped villi (SV); dome-shaped synoviocytes (S); deep synoviocytes (DS); scratched surface (Sr); dense irregular fibers (DI)

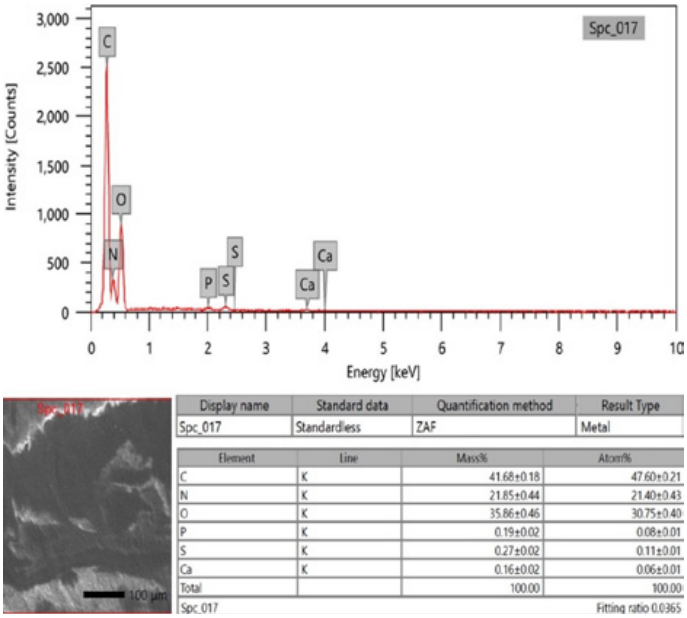

Display name	Standard data	Quantification method	Result Type
Spc_017	Standardless	ZAF	Metal

Element	Line	Mass%	Atom%
C	K	41.68±0.18	47.60±0.21
N	K	21.85±0.44	21.40±0.43
O	K	35.86±0.46	30.75±0.40
P	K	0.19±0.02	0.08±0.01
S	K	0.27±0.02	0.11±0.01
Ca	K	0.16±0.02	0.06±0.01
Total		100.00	100.00

Spc_017 Fitting ratio 0.0365

Figure 10: SEM-EDX image explaining the components at the menisci of the horse's stifle joint

The elemental composition demonstrated the following mass concentration hierarchy: carbon> oxygen > nitrogen > sulfur > phosphorus > calcium

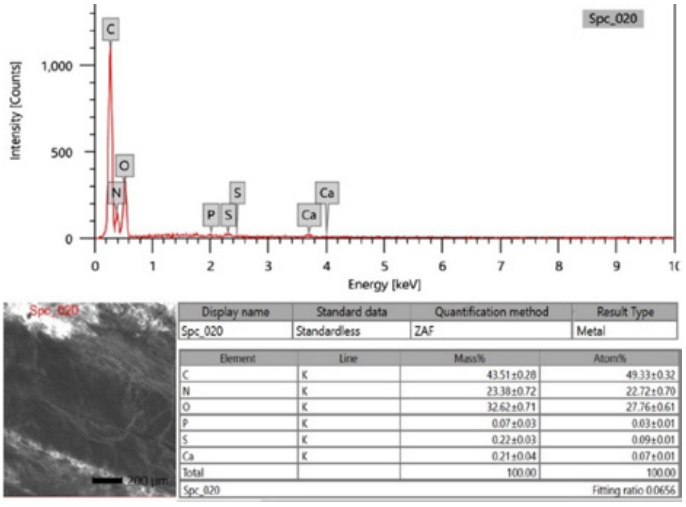

Display name	Standard data	Quantification method	Result Type
Spc_020	Standardless	ZAF	Metal

Element	Line	Mass%	Atom%
C	K	43.51±0.28	49.33±0.32
N	K	23.38±0.72	22.72±0.70
O	K	32.62±0.71	27.76±0.61
P	K	0.07±0.03	0.03±0.01
S	K	0.22±0.03	0.09±0.01
Ca	K	0.21±0.04	0.07±0.01
Total		100.00	100.00

Spc_020 Fitting ratio 0.0656

Figure 11: SEM-EDX image explaining the components of the patellar ligaments of the horse's stifle joint

The elemental composition demonstrated the following mass concentration hierarchy: carbon > oxygen > nitrogen > sulfur > calcium > phos-phorus

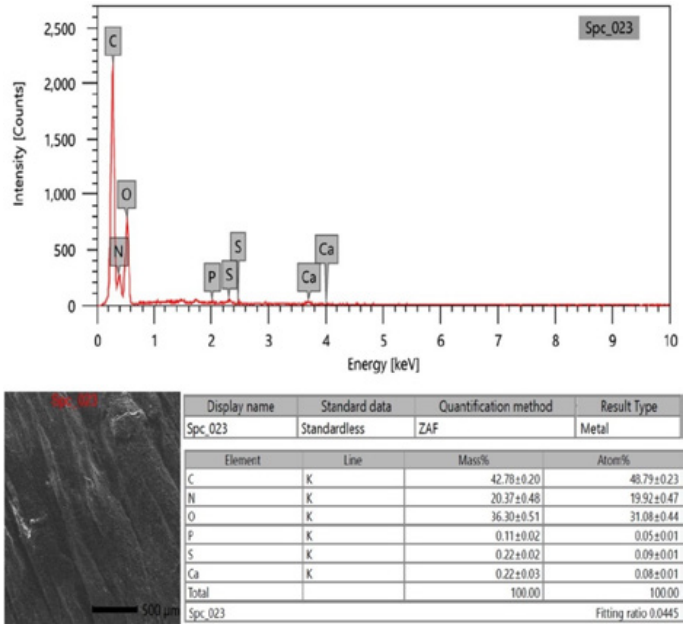

Display name	Standard data	Quantification method	Result Type
Spc_023	Standardless	ZAF	Metal

Element	Line	Mass%	Atom%
C	K	42.78±0.20	48.79±0.23
N	K	20.37±0.48	19.92±0.47
O	K	36.30±0.51	31.08±0.44
P	K	0.11±0.02	0.05±0.01
S	K	0.22±0.02	0.09±0.01
Ca	K	0.22±0.03	0.08±0.01
Total		100.00	100.00
Spc_023			Fitting ratio 0.0445

Figure 12: An SEM-EDX image explaining the components of the cruciate ligaments of the horse's stifle joint

The elemental composition demonstrated the following mass concentration hierarchy: carbon > oxygen > nitrogen > sulfur > calcium > phos-phorus.

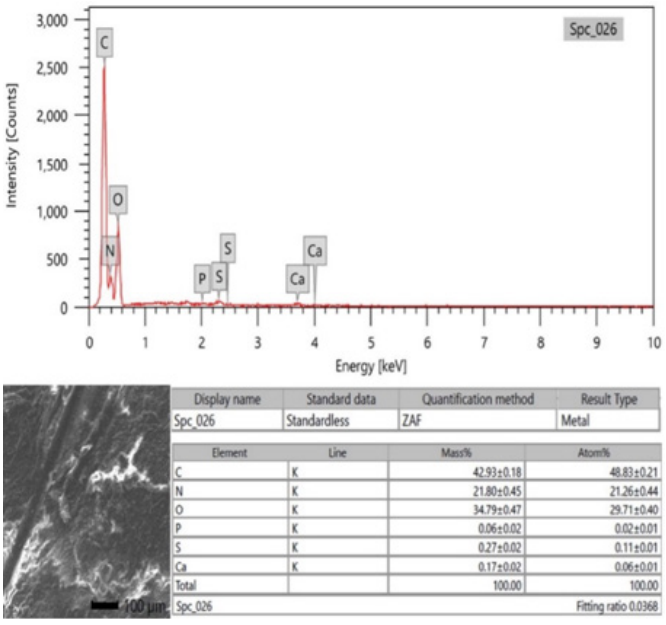

Display name	Standard data	Quantification method	Result Type
Spc_026	Standardless	ZAF	Metal

Element	Line	Mass%	Atom%
C	K	42.93±0.18	48.83±0.21
N	K	21.80±0.45	21.26±0.44
O	K	34.79±0.47	29.71±0.40
P	K	0.06±0.02	0.02±0.01
S	K	0.27±0.02	0.11±0.01
Ca	K	0.17±0.02	0.06±0.01
Total		100.00	100.00
Spc_026			Fitting ratio 0.0368

Figure 13: SEM-EDX image explaining the components of the collateral ligaments of the horse's stifle joint

The elemental composition demonstrated the following mass concentration hierarchy: carbon > oxygen > nitrogen > sulfur > calcium > phos-phorus

Table 1: The mass percentage and mean ± standard error of various elements in the menisci, patellar ligaments, cruciate ligaments, and collateral ligaments

	Menisci		Patellar ligament		Cruciate ligament		Collateral ligament	
	Horse1	**Horse2**	**Horse1**	**Horse2**	**Horse1**	**Horse2**	**Horse1**	**Horse2**
C	42.04±0.18	41.68±0.18	43.51±0.28	39.41±0.21	42.78±0.20	41.16±0.26	42.93±0.18	38.74±0.30
O	36.05±0.46	35.86±0.46	32.62±0.71	36.41±0.56	36.30±0.51	35.51±0.68	34.79±0.47	36.11±0.82
N	21.45±0.43	21.85±0.44	23.38±0.72	23.89±0.52	20.37±0.48	22.86±0.64	21.80±0.45	24.88±0.76
S		0.16±0.02	0.22±0.03	0.19±0.02	0.22±0.02	0.22±0.03	0.27±0.02	0.10±0.03
Ca	0.25±0.02	0.27±0.02	0.21±0.04	0.11±0.02	0.22±0.03	0.16±0.03	0.17±0.02	0.12±0.03
P	0.03±0.01	0.19±0.02	0.07±0.03		0.11±0.02	0.09±0.02	0.06±0.02	0.04±0.02
Si	0.18±0.02							
Ca+p	0.25	0.46	0.27	0.11	0.33	0.25	0.23	0.16

produced excellent 3D images of bones with large and small bony structures and soft structures. The 3D render volume of CT images of the bones and joints helps assess the typical fractures and dislocations (23, 39, 40, 41, 51). 3D reconstruction images improve the approach and understanding of bone anatomy and can value related diseases, allowing radiologists to identify and demonstrate individual os-seous and soft-tissue components of complex anatomy (19, 52, 53). The 3D image can be transferred to an anatomical modal cast using a 3D printer, simplifying and improving the learning process while benefiting research and diagnosis (54). CT image reconstruction into three dimensions enhances bone and joint contour assessment and delineation of fracture orientation or bone fragmentation (55, 56).

The complex stifle joint consisted of three main joint sacs: fem-oropatellar, medial, and lateral femorotibial. The ligaments of the stifle joint and meniscus were determined using a 3D reconstruc-tion CT, which provided a well-defined baseline reference image for donkey stifle joints (57).

Our study's sagittal CT sections and subsequent CT bone window cross sections provided detailed images of the bone's structures, ligaments, and muscles. The sectional CT sections were com-pared to cross and sagittal anatomical sections. The images supplied should increase the clinical use of CT to diagnose patho-logical conditions within the stifle joint that cause clinical lameness. CT scans are beneficial for evaluating menisci and cruciate ligaments (18, 58, 59, 60). CT of the equine stifle joint has shown promise as a clinically helpful technique for stifle joint injury de-tection, such as injury to the meniscus, cranial tibial ligaments of the lateral and medial menisci, and cruciate ligaments has been recognized (61). (62) used 3D radio stereometric analysis and equine cadaver stifles to determine the functional range of mo-tion. Understanding the normal kinematics of the equine stifle and the relationship between joint positions and articular contact areas may shed light on the etiology and location of common stifle joint pathologies (meniscal lesions and articular). Stifle joint injuries (meniscus and ligaments) are becoming more common in equines (63).

SEM revealed that the synovial villi varied in length, had two types, long and short, with varying tip shapes, and contained dome-shaped synoviocytes. The rest of the surface featured single or branched folds. Pig, rabbit, and rat knee joints showed blunt processes on their synovial villous surfaces (64). The char-acter of donkey carpal synovial villi exhibits the longer villi that were branched in their tips at the horse carpal (22), they were densely arranged and were longer than those of other mammals and had two types of synoviocytes; the upper half of the villi had protruded an antenna-like process into the joint cavity with tips covered with long microvilli (23). In the calf antebrachiocarpal joint, the synovial membrane consisted of type A synoviocytes that were located adjacent to the joint lumen (65). In the synovial membrane of the rabbit knee joint in the case of osteoarthritis, both types of synoviocytes increased in number and changed their morphology, indicating their elevated activities in absorp-tion and secretion (22, 23, 65, 66). Cells are abundant in synovial villi and folds and are primarily exposed to the joint cavity; they help maintain joint cavity homeostasis by phagocytosing waste and cell debris in the synovial fluid (64) in horse, (67) in human, (68) in White Leghorn chicken embryos.

Deep synoviocytes appeared at the scratched membrane; dis-tinguish between superficial and deep synoviocytes. (69) in eq-uine described the existence of multiple layers of synovial cells surrounding a dense fibrous core. The synovial membrane had two types of synoviocytes; type A-synoviocytes were spherical and possessed many processes, while type B-synoviocytes pre-sented at the luminal synovial surfaces (22, 64) in the horse, (70) in rats, rabbits, dwarf goats, sheep, pig, dog, and human. The lamina propria was dense and irregular in our sample, while the synovial membrane comprised synovial cells and lamina propria of various types: areolar, adipose, and fibrous; a similar observa-tion was stated by (69) in horse. Scanning electron microscopy revealed that human adipose and areolar tissue have a surface pattern, and blunt processes cover synovial villi (70) in human, pig, rat, and rabbit. The synovial membrane was covered with closely arranged synovial villi; other areas of the synovial membrane's surface had folded synovial membrane; the folds were either single or branched, and there were four types of gross construction at the synovial membrane of rabbit knee: accordi-on-like, lobe-like, fatty areolar, and flattened areas (71) in rabbit.

SEM-EDX detected carbon, oxygen, nitrogen, sulfur, calcium, and phosphorus in the menisci and various ligaments of the stifle joint. Selenium was replaced by sulfur in the menisci, and calcium and phosphorus were trace amounts, with the menisci having the highest percentage and the collateral and patellar ligaments having the lowest. The percentage of sulfur was also trace; liga-ments had the highest percentage compared to menisci (28). The calcium, sulfur, and phosphorus content of ligaments and tendons generally showed some exciting differences. Furthermore, sig-nificant regional variations may be associated with the presence or absence of fibrocartilage in the "wraparound." The sulfur and calcium concentrations are incredibly high, which is undoubtedly linked to elevated levels of proteoglycans (28).

The tendons and ligaments have different chemical properties. There were also more minor differences between ligaments and tendons. The findings indicate that ligaments are metabolically more active than tendons. They also have less total collagen than tendons but more glycosaminoglycans—relatively increased ligament metabolic activity (26). The relative contents of sulfur, calcium, and phosphorus in human menisci increased gradually and then decreased (72). Age-related changes in the trace ele-ment content of tendons and ligaments can aid in interpreting and evaluating morphological and biochemical changes in tissues and mechanical properties (26, 28).

Silicon plays a vital role in connective tissue, with the primary effect on bone and cartilage appearing to be the formation of the organic matrix. As a result, silicon is now required to form colla-gen and glycosaminoglycan. Silicon is involved in the biochemis-try of subcellular enzyme-containing structures and has essential interactions with other elements. The link between silicon and aging is likely due to glycosaminoglycan changes (73).

Conclusion

CT, sectional anatomy, SEM, and SEM-EDX analysis described the horse's stifle joint. The 3D render volume reconstruction CT enables clear viewing of the large and small bone features, ligaments, and meniscus. Understanding the stifle joint's macro- and microscopic normal anatomy acquired by 3D CT, SEM, and SEM-EDX is a valuable tool and reference for assessing the horse stifle's bone and soft tissue structures and microstructures

Acknowledgements

We thank Alexandria and Damanhour Universities for their help in completing this work.

Ethics approval. The study complied with the ARRIVE guidelines and followed the U.K. Animals (Scientific Procedures) Act, 1986, and associated guidelines, EU Directive 2010/63/EU for animal experiments.

All methods followed relevant guidelines and regulations with ethical permission from the Alexandria University Research Ethics Review Committee of the Faculty of Veterinary Medicine, Alex-andria University (*Approval No: Au/13/04/03/2024/096*).

We obtained informed consent and permission from the Depart-ment of Anatomy and Embryology, Faculty of Veterinary Medi-cine, Alexandria University, to use the hind limbs of euthanized horses in our study.

Availability of data and materials. The datasets used and/or analyzed during the current study are available from the corre-sponding author upon reasonable request.

Declaration of Competing Interest. The authors declare that they have no known competing financial interests or personal rela-tionships that could have appeared to influence the work report-ed in this paper.

Funding. The current study does not have any funds from any organizations or institutions.

Authors' contributions. MAMA, AKSE, and SAAE wrote the man-uscript and interpreted the results; MAMA, AKSE, IA, and AGN collected the samples and performed the CT scanning; MAMA, AKSE, and SAAE collected the samples and performed the scan-ning electron microscopy; MAMA and SAAE prepared the fig-ures, and IA and AGN assisted in interpreting the results.

Abbreviations: Computed Tomography (CT), 3D Computed To-mography (3D CT), Scanning Electron Microscopic (SEM), Scan-ning electron microscopy-Energy Dispersive X-Ray Analysis (SEM-EDX), Carbon, Oxygen, Nitrogen, Sulfur, Calcium, Phosphorus, and Silicon (C, O, N, S, Ca, P, and Si).

References

1. Carpenter Jr D, Cooper R. Mini review of canine stifle joint anatomy. Anat Histol Embryol 2000; 29 (6): 321–9.
2. Budras KD, Sack WO, Rock S, Horowitz A, Berg R. Anatomy of the Horse, Sixth Edition: Schluetersche, Germany; 2012.
3. Walmsley JP. Diagnosis and treatment of ligamentous and meniscal injuries in the equine stifle. Vet Clin North Am Equine Pract 2005; 21 (3): 651–72.
4. Judy C. The stifle. Equine MRI 2010:451-466.
5. Moore KW, Read RA. Rupture of the cranial cruciate ligament in dogs-part I. Compend Contin Educ Vet 1996; 18 (3): 223–33.
6. Jeffcott L, Kold S. Stifle lameness in the horse: a survey of 86 referred cases. Equine Vet J 1982; 14 (1): 31–9.
7. Stashak TS. Adams' lameness in horses, 4th edn: Verlag M. & H. Schaper; 2008.
8. Dyson SJ. Lameness associated with the stifle and pelvic regions. In: Proceedings of the Annual Convention of the AAEP. 2002: 387–411.
9. Jeffcott L. Interpreting radiographs 3: radiology of the stifle joint of the horse. Equine Vet J 1984; 16 (2): 81–8.
10. Butler J, Colles C, Dyson S, Kold S, Poulos P. The stifle and tibia. Clinical radiology of the horse . Ames: Wiley Blackwell, 2000:363–412.
11. McIlwraith CW, Frisbie DD, Kawcak CE, Van Weeren R. Joint disease in the horse. Amsterdam: Elsevier, 2015.
12. McIlwraith CW, Kawcak C, Baxter GM, Goodrich LR, Valberg SJ. Principles of musculoskeletal disease: joint injuries and disease and osteoarthritis. In: Baxter GM, ed. Adams and Stashak's Lameness in Horses. 7th ed. Hoboken: Wiley, 2020: 801–74.
13. Marino DJ, Loughin CA. Diagnostic imaging of the canine stifle: a review. Vet Surg 2010; 39(3): 284–95.
14. Antonacci JM, Schmidt TA, Serventi LA, et al. Effects of equine joint injury on boundary lubrication of articular cartilage by synovial fluid: role of hyaluronan. Arthritis Rheum 2012; 64(9): 2917–26.
15. Denoix J-M. Essentials of clinical anatomy of the equine locomotor system. Boca Raton: CRC press, 2019.
16. Badawy AM. Computed tomographic anatomy of the fore foot in one-humped camel (Camelus dromedrus). Glob Vet 2011; 6(4): 417–23.
17. Alsafy M, El-Kammar M, El-Gendy S. Topographical anatomy, computed tomography, and surgical approach of the guttural pouches of the donkey. J Equ Vet Sci 2008; 28 (4): 215–22.
18. Van der Vekens E, Bergman EH, Vanderperren K, et al. Computed tomographic anatomy of the equine stifle joint. Am J Vet Res 2011; 72(4): 512–21.
19. El-Gendy SA, Kamal BM, Alsafy MA. 3D render volume CT reconstruction of the bones and arteries of the hind digit of the dromedary camel (Camelus dromedarius). BMC Zool 2022; 7(1): 49.
20. El-Gendy SA, Alsafy MA, Rutland CS, Ez Elarab SM, Abd-Elhafeez HH, Kamal BM. Ossa cordis and os aorta in the one-humped camel: Computed tomography, light microscopy and morphometric analysis. Microscopy Research and Technique 2023, 86 (1):53-62.
21. El-Gendy SA, Alsafy MA, Rutland CS, El-Khamary AN, Abu-Ahmed HM, El-Kammar MH. Morphological and imaging evaluation of the metacarpophalangeal and metatarsophalangeal joints in healthy and lame donkeys. J Equ Vet Sci 2020; 88: 102904. doi: 10.1016/j.jevs.2019.102904

22. Shikichi M, Kitamura HP, Yanase H, Konno A, Takahashi-Iwanaga H, Iwanaga T. Three-dimensional ultrastructure of synoviocytes in the horse joint as revealed by the scanning electron microscope. Arch Histol Cytol 1999; 62(3): 219–29.

23. Alsafy MA, El-Gendy SA, Abou-Ahmed HM. The carpal joint of the donkey (Equus asinus): morphological investigation. Internat J Morphol 2015; 33(3): 948-54.

24. Fugazzola M, Nissinen MT, Jäntti J, et al. Composition, architecture and biomechanical properties of articular cartilage in differently loaded areas of the equine stifle. Equine Vet J 2024; 56(3): 573–85.

25. White JL, Salinas EY, Link JM, Hu JC, Athanasiou KA. Characterization of adult and neonatal articular cartilage from the equine stifle. J Equine Vet Sci 2021; 96: 103294. doi: 10.1016/j.jevs.2020.103294

26. Amiel D, Frank C, Harwood F, Fronek J, Akeson W. Tendons and ligaments: a morphological and biochemical comparison. J Orthop Res 1983; 1(3): 257–65.

27. Edwards J. The nature and origins of synovium: experimental approaches to the study of synoviocyte differentiation. J Anat 1994; 184 (3): 493–501.

28. Kumai T, Yamada G, Takakura Y, Tohno Y, Benjamin M. Trace elements in human tendons and ligaments. Biol Trace Elem Res 2006; 114(1/3): 151–61.

29. Thorpe CT, Screen HR. Tendon structure and composition. Adv Exp Med Biol 2016; 920: 3-10.

30. Ribitsch I, Peham C, Ade N, et al. Structure—Function relationships of equine menisci. PLoS One 2018; 13(3): e0194052. doi: 10.1371/journal.pone.0194052

31. Penninck DG, Nyland TG, O'Brien TR, Wheat JD, Berry CR. Ultrasonography of the equine stifle. Vet Radiol 1990; 31(6): 293–8.

32. El Sharaby AA, Alsafy MA, El-Gendy SA. Equine anatomedia: development, integration and evaluation of an e-learning resource in applied veterinary anatomy. Int J Morphol 2015; 33(4): 1577-84.

33. Holcombe SJ, Bertone AL, Biller DS, Haider V. Magnetic resonance imaging of the equine stifle. Vet Radiol Ultrasound 1995; 36(2): 119–5.

34. Hoegaerts M, Nicaise M, van Bree H, Saunders J. Cross-sectional anatomy and comparative ultrasonography of the equine medial femorotibial joint and its related structures. Equine Vet J 2005; 37(6): 520–9.

35. Maulet BEB, Mayhew I, Jones E, Booth T. Radiographic anatomy of the soft tissue attachments of the equine stifle. Equine Vet J 2005; 37(6): 530–5.

36. Dyce KM, Sack WO, Wensing CJG. Textbook of Veterinary Anatomy. St. Louis: Mosby, 2010.

37. Ali S, Esmat A, Erasha A, Yasuda M, Alsafy M. Morphology and morphometry of the inner ear of the dromedary camel and their influence on the efficiency of hearing and equilibrium. Zoo Lett 2022; 8(1): 1-12. doi: 10.1186/s40851-022-00196-0

38. Alsafy MA. Comparative morphological studies on the lacrimal apparatus of one humped camel, goat, and donkey. J Biol Sci 2010; 10(3): 224–30. doi: 10.3923/jbs.2010.224.230

39. Alsafy MA, El-Gendy SA, Kamal B. Morphological, radiographic and computed tomographic evaluation of the metatarsophalangeal joint of the one-humped camel. Anat Histol Embryol 2018; 47(6): 537–43.

40. Alsafy MA, El-Gendy SA, Kamal B. Computed tomographic and radiographic morphology of the pastern and coffin joints of One-Humped Camel (Camelus dromedarius). Anat Histol Embryol 2021; 50(1): 108–13.

41. Alsafy MAM. Computed tomography and cross-sectional anatomy of the thorax of goat. Small Rum Res 2008; 79(2/3): 158–66.

42. El-Gendy S, Alsafy M, El Sharaby A. Computed tomography and sectional anatomy of the head cavities in donkey (Equus asinus). Anat Sci Int 2014; 89(3): 140–50.

43. Alsafy MA, El-Gendy SA. Morphological investigation of the gills of the dusky grouper Epinephelus marginatus (Lowe 1834) using gross anatomy and scanning electron microscopy. Microsc Res Tech 2022; 85(5): 1891–8.

44. Alsafy MA, Seif MA, El-Gendy SA, El-Beskawy M, El Dakroury M. Ultrastructure of the oropharyngeal cavity floor of the red porgy (Pagrus pagrus) by light and scanning electron microscopy. Microsc Microanal 2023; 29(1): 273–82.

45. Ez Elarab SM, El-Gendy SA, El-Bakary NE, Alsafy MA. Ultrastructure of the palatine tonsils of the donkey (Equus asinus): new insights by light, scanning, and transmission electron microscopy. Microsc Res Tech 2022; 85(12): 3793–803.

46. El-Bakary NE, Alsafy MA, El-Gendy SA, Elarab SME. New insights into the retinal microstructure-diurnal activity relationship in the African five-lined skink (Trachylepis quinquetaeniata) (Lichtenstein, 1823). Zoological Lett 2023; 9(1) : 7. doi: 10.1186/s40851-023-00205-w

47. Alsafy M, El-Gendy S. Gastroesophageal junction of Anatolian shepherd dog; a study by topographic anatomy, scanning electron and light microscopy. Vet Res Commun 2012; 36(1): 63-9.

48. El-Gendy SAA, Derbalah A, El-Mansi AA, El Okle OS, Alsafy MAM. Light and scanning electron microscopic characterization of the Egyptian buffalo hair in relation to age with analysis by SEM-EDX. Microsc Res Tech 2023; 86(8): 955–65. doi: 10.1002/jemt.24366

49. Derbalah A, El-Gendy SA, Alsafy MA, Elghoul M. Micro-morphology of the retina of the light-adapted African catfish (Clarias gariepinus). Microsc Res Tech 2023; 86(2): 208–15.

50. Rashwan AM, El-Gendy SAA, Alsafy MAM, Haddad SS. Comparative morphological analysis of telson and uropods in Penaeus canaliculatus (Olivier, 1811), Penaeus semisulcatus (De Haan, 1844), and Metapenaeus stebbingi (Nobili, 1904) using scanning electron microscopy and EDX analysis. Micron 2024; 181: 103636. doi: 10.1016/j.micron.2024.103636

51. Rózyło-Kalinowska I, Rózyło T. Diagnostic algorithm in high (cranial) maxillofacial fractures. Ann Univ Mariae Curie Sklodowska Med 2000; 55: 309-17.

52. Alsafy MA, Elbakary RM, Bassuoni NF. A study of the shoulder and elbow joints of the donkey (Equus asinus) by gross anatomical dissection, radiography, computed tomography, and intra-articular injection. Morphologie 2022; 106(354): 177-87.

53. Fatterpekar GM, Doshi AH, Dugar M, Delman BN, Naidich TP, Som PM. Role of 3D CT in the evaluation of the temporal bone. Radiographics 2006; 26 (suppl. 1): S117-S132.

54. Jáber Mohamad JR, Carrascosa Iruzubieta CJ, Arencibia Espinosa A, Corbera Sánchez JA, Ramírez Corbera AS, Melián Limiñana C. 3-D computed tomography reconstruction: another tool to teach anatomy in the veterinary colleges. Iran J Vet Res 2018.

55. Davidson E, Ross M, Parente E. Incomplete sagittal fracture of the talus in 11 racehorses: outcome. Equine Vet J 2005; 37(5): 457–61.

56. Kelmer G, Wilson D, Essman S. Computed tomography assisted repair of a central tarsal bone slab fracture in a horse. Equine Vet Educ 2008; 20(6): 284–7.

57. Abumandour MM, Bassuoni NF, El-Gendy S, Karkoura A, El-Bakary R. Cross-anatomical, radiographic and computed tomographic study of the stifle joint of donkeys (Equus africanus asinus). Anat Histol Embryol 2020; 49(3): 402–16.

58. Buckwalter KA. Current concepts and advances: computerized tomography in sports medicine. Sports Med Arthrosc Rev 2009; 17(1): 13-20.

59. Buckwalter KA. CT arthrography. Clin Sports Med 2006; 25(4): 899–915.

60. Mutschler C, Vande Berg BC, Lecouvet FE, et al. Postoperative meniscus: assessment at dual–detector row spiral CT arthrography of the knee. Radiology 2003; 228(3): 635–41.

61. Bergman HJ, Saunders J. Equine upper limbs (carpus, tarsus, stifle). Vet Comp Tomography2011:483-501.

62. Halley S, Bey M, Haladik J, Lavagnino M, Arnoczky S. Three dimensional, radiosteriometric analysis (RSA) of equine stifle kinematics and articular surface contact: a cadaveric study. Equine Vet J 2014; 46(3): 364–9.

63. Walmsley J, Phillips T, Townsend H. Meniscal tears in horses: an evaluation of clinical signs and arthroscopic treatment of 80 cases. Equine Vet J 2003; 35 (4): 402–6.

64. Iwanaga T, Shikichi M, Kitamura H, Yanase H, Nozawa-inoue K. Morphology and functional roles of synoviocytes in the joint. Arch Histol Cytol 2000; 63(1): 17-31.

65. Leach DH, Caldwell SJ, Ferguson JG. Ultrastructural study of synovial membrane from the antebrachiocarpal joint of calves. Cells Tissues Organs 1988; 133 (3): 234–46.

66. Nio J, Yokoyama A, Okumura M, Iwanaga T. Three-dimensional ultrastructure of synoviocytes in the knee joint of rabbits and morphological changes in osteoarthritis model. Arch Histol Cytol 2002; 65(2): 189–200.

67. Esposito CI. Wear in ceramic-on-ceramic total hip replacements: mechanisms and implications of edge loading. Sydney: UNSW Sydney, 2012. doi: 10.26190/unsworks/15983

68. Williams R. Effects of mechanical strain hyaluronan metabolism of synovial cells from osteoarthritic knees. Cardiff: Cardiff University, 2004. Doctoral thesis. https://orca.cardiff.ac.uk/id/eprint/55950/

69. Updike SJ, Diesem CD. Histologic appearance and distribution of synovial membrane types in the equine stifle joint. Anat Histol Embryol 1983; 12(1): 53–9.

70. Woodward D, Gryfe A, Gardner D. Comparative study by scanning electron microscopy of synovial surfaces of four mammalian species. Experientia 1969; 25 (12): 1301–3.

71. Levanon D, Stein H. The synovial lining of the rabbit knee: a scanning electron microscopy study of specimens reinforced structurally with tannic acid. Histochem J 1992; 24: 25–32.

72. Moriwake Y, Tohno Y, Tohno S, et al. Age-related changes of element contents in the human meniscus. Biol Trace Elem Res 1998; 64: 229–35.

73. Carlisle EM. Silicon as a trace nutrient. Sci Total Environ 1988; 73(1/2): 95–106.

Nova spoznanja o konjskem kolenskem sklepu s pomočjo 3D-računalniške tomografije, vrstične elektronske mikroskopije ter vrstične elektronske mikroskopije in energijsko disperzijske rentgenske analize

M. A.M. Alsafy, A. K.S. El-Garhy, I. Abo-Ghanima, A. G. Nomir, S. A.A. El-Gendy

Izvleček: Zasnova študije konjskega kolenskega sklepa je bila prospektivna in opisna, z uporabo CT, anatomije iz rezin, SEM in analize EDX. CT konjskega kolenskega sklepa z rekonstrukcijo tridimenzionalnega upodobljenega volumna omogoča dobro vizualizacijo velikih in majhnih kostnih struktur ter vezi ali meniskusov. Poleg sagitalnih CT-rezin in naknadnih prečnih CT-rezin kosti, ki so omogočile podrobne posnetke kostnih struktur, vezi in mišic, so bili sekcijski CT-ji usklajeni s prečnimi in sagitalnimi anatomskimi prerezi. Konjski kolenski sklep je opisan z analizo SEM in EDX. Sinovialna membrana je imela različne sinovialne resice po dolžini in obliki: dolge in kratke jezičaste z različnimi konicami in kupolasto obliko, poleg tega pa tudi posamezne ali razvejene gube. Površina razkriva mrežo kolagenih vlaken, razporejenih v različnih smereh, plasteh in globoke sinoviocite. Spektri SEM-EDX so identificirali naslednje elemente v meniskusih in vezeh kolenskega sklepa: vzorec je vseboval ogljik, kisik, dušik, žveplo, kalcij in fosfor, pri čemer je selen v meniskusu zamenjal žveplo. Pregledali smo štiri vzorce, da bi določili odstotni delež ogljika in kisika. Izmerjene so bile vrednosti kalcija in fosforja, pri čemer so bile najvišje koncentracije v meniskusu, najnižje pa v kolateralnih in patelarnih vezeh. Določen je bil odstotek žvepla, ki je bil v ligamentih višji kot v meniskusih, zlasti v križnih vezeh, medtem ko so meniskusi vsebovali silicij. Poznavanje normalne makro- in mikroskopske anatomije kolenskega sklepa, pridobljene s 3D-CT, SEM in EDX, je dobro vodilo in referenca za določanje kostnih in mehkotkivnih struktur in mikrostruktur ter kemične strukture sinovialne membrane, ligamentov in meniskusov konjskega kolenskega sklepa.

Ključne besede: konj; kolenski sklep; 3D-CT; anatomska analiza iz rezin; SEM; SEM-EDX